12-15-2014

Quantifying Individual Losses in a Direct Methanol Fuel Cell

Jennifer Rae Ruffing
University of South Carolina - Columbia

QUANTIFYING INDIVIDUAL LOSSES IN A DIRECT METHANOL FUEL CELL

by

Jennifer Rae Ruffing

Bachelor of Science
Florida Institute of Technology, 2007

Submitted in Partial Fulfillment of the Requirements

For the Degree of Master of Science in

Chemical Engineering

College of Engineering and Computing

University of South Carolina

2014

Accepted by:

John Weidner, Director of Thesis

Xinyu Huang, Reader

Michael Matthews, Reader

Lacy Ford, Vice Provost and Dean of Graduate Studies

DEDICATION

I dedicate this thesis to my family. To my amazing mother, who inspires me daily and who instilled a love of learning in me that I hope to pass on to my own children. To my father, who encouraged my love of math and science from such a young age. To my sister, Dani, who always keeps me laughing and is my very best friend. And to my beautiful daughter, Arabella Grace. You are the best thing that's ever happened to me, and I love you more than you will ever know.

Finally, I dedicate this work to my wonderful husband, Colby. Thank you for supporting me through this journey, for encouraging me no matter what, and for pushing me to follow my dreams. I love you, and I couldn't have done this without you.

ACKNOWLEDGEMENTS

I would like to sincerely thank my advisor, Dr. John Weidner, for his guidance and support throughout this study, and especially for his patience with me. He never gave up on me, and I will always be grateful for his advice and understanding. I'd also like to thank Dr. Brenda Garcia, who guided and inspired me throughout this journey. I learned so much from her and am grateful for all of her assistance throughout my time at USC, as well as for her friendship. And to Carol Stork, I offer my sincere gratitude for her help and kindness in my initial research and data interpretation.

To all of my friends and classmates, thank you for your understanding and encouragement along the way. There are so many of you who had an impact on this work, both from the REU program and throughout graduate school, and I can never thank you enough.

Finally, a huge thank you to my family, for your endless love, support, and encouragement, and for giving me strength to reach for the stars and chase my dreams. I love you all so much.

ABSTRACT

The performance of a direct methanol fuel cell (DMFC) is complicated due to the complex interactions of kinetic and transport processes. As a result, changes in one aspect of the cell have consequences in other aspects, which are difficult to elucidate from the full-cell polarization (i.e. voltage vs. current) behavior that fuel cell researchers often use to characterize the performance of their systems. The objective of this work was to develop a strategy to use current and voltage relationships from anode half cells, cathode half-cells, and a hydrogen pump, coupled with methanol crossover data and a mathematical model, to quantify the individual losses within a DMFC. In this way, all the kinetic and transport processes are quantified and the cell voltage can be deconstructed (i.e. individual voltage losses quantified). This data analysis accounts for all of the voltage losses observed during the operation of the full cell. As expected, the anode and cathode overpotentials accounted for most of the losses (i.e. 92% average). Also, the cathode flow rate has been shown to affect the methanol crossover by diffusion. Cells operated at constant stoichiometry or where the cathode flow rate is small can show a parabolic shape in the methanol crossover because the electroosmotic drag dominates over diffusion as the primary transport mechanism for methanol through the membrane. Decrease in the methanol crossover was observed for cells with high compression and thicker cathode electrodes. The one-dimensional model, developed previously [1], was improved by including: (1) methanol transport from the anode flow channel to the backing layer using a mass transfer resistance; and (2) accounting for the unreacted

methanol transport through the cathode. The model was able to reasonably predict the anode, cathode, full-cell polarization, and methanol crossover data for methanol concentrations between 0.05 M and 2 M at all operating currents.

TABLE OF CONTENTS

LIST OF TABLES

LIST OF FIGURES

LIST OF SYMBOLS

A_{Cross}	cross-section area, cm^2
a	specific surface area of the anode, cm^{-1}
c_0^B	concentration of methanol at the anode flow channel/ABL interface, mol/cm^3
c	concentration, mol/cm^3
c_{MeOH}	concentration of methanol, mol/cm^3
c_{O_2}	concentration of oxygen, mol/cm^3
D_A	effective diffusion coefficient of methanol in the ACL, cm^2/s
D_B	effective diffusion coefficient of methanol in the ABL, cm^2/s
D_H	hydraulic diameter, cm
D_M	effective diffusion coefficient of methanol in the membrane, cm^2/s
D_{MeOH}	stream diffusion coefficient of methanol in the anode flow channel, cm^2/s
F	Faraday's constant, 96,487 C/equiv
i_{Cell}	cell current density, A/cm^2
i_{Leak}	leakage current density due to methanol crossover, A/cm^2
$i_{0,ref}^{MeOH}$	exchange current density of methanol, A/cm^2
$i_{0,ref}^{O_2}$	exchange current density of oxygen, A/cm^2

k	constant in the anode kinetic expression, dimensionless
k_{Ch}	mass transfer coefficient in the anode flow channel, cm/s
k_C	mass transfer coefficient in the cathode backing layer, cm/s
ℓ_{Ch}	length of the anode flow channel, cm
$N_{z,MeOH}$	z component of methanol molar flux, mol/(cm^2 s)
n_{Ch}	number of parallel channels in the graphite block, dimensionless
P_{Wet}	wet perimeter, cm
Q_C	volumetric flow rate in the cathode flow channel, cm^3/s
R	gas constant, 82.06 (cm^3 atm)/(mol K) or 8.314 J/ (mol K)
R_M	Resistance of membrane, Ω
R_{Ion}	Resistance of ionomer, Ω
s	stoichiometric coefficient
T	temperature, K
U^{MeOH}	thermodynamic equilibrium potential of methanol oxidation, V
U^{O_2}	thermodynamic equilibrium potential of oxygen oxidation, V
V_{Cell}	cell voltage, V
v	velocity in anode flow channel, cm/s
w_{Ch}	width of the anode flow channel, cm
x_{MeOH}	mole fraction of methanol, mol/mol
z	coordinate direction normal to the anode, cm

Greek

α_A	anodic transfer coefficient
α_C	cathodic transfer coefficient
δ_A	ACL thickness, cm
δ_B	ABL thickness, cm
δ_{Ch}	depth of anode flow channel, cm
δ_M	membrane thickness, cm
η	overpotential, V
κ	ionic conductivity of the membrane, S/cm
λ	constant in the anode kinetic expression, mol/cm^3
μ	viscosity, g/cm s
ρ	density, g/cm^3
ξ_{MeOH}	electro-osmotic drag coefficient of methanol

LIST OF ABBREVIATIONS

A.....ACL

B.....ABL

Cell.....cell

Ch..... anode flow channel

exp.....experimental

H2..... hydrogen

I ..... ABL/ACL interface

II.....ACL/membrane interface

III..... membrane/cathode layer interface

Ion .....electrode ionomer

IR.....ohmic resistance

M.....membrane

MeOH .....methanol

O2.....oxygen

ox.....oxidation reaction

red .....reduction reaction

X-over ..... methanol crossover

z..... z-direction

CHAPTER 1

GENERAL INTRODUCTION

Direct Methanol Fuel Cells (DMFCs) have significant voltage losses in both the anode and cathode due to the slow kinetics of methanol oxidation and oxygen reduction, respectively, and substantial loss of methanol across the membrane (i.e. methanol crossover). The complex interactions of these transport and kinetic losses complicate the process of isolating these phenomena and quantifying the effect of components (e.g. catalysts, membrane, backing layer), cell assembly (e.g. clamping pressure), and operating conditions (e.g. temperature, methanol concentration, flow rate). Understanding the magnitude of the individual losses in a DMFC provides the opportunity to optimize cell design and operating conditions and to understand the interactions between the anode and the cathode.

Extensive work has been done to understand the DMFC behavior and to address the two major effects: methanol oxidation kinetics and methanol crossover. Reviews in these subjects can be found elsewhere [2-4]. In order to improve the methanol oxidation kinetics several catalysts have been explored [5]. The most common catalysts used for the methanol oxidation at the anode are based on Pt-Ru. Research has focused on synthesis of bimetallic particles [6, 7], optimization of the support [8-10], the catalyst particle size [11, 12] and the atomic ratio [13, 14]. However, in the search for more active and less expensive catalysts than Pt-Ru, researchers have also evaluated non-Pt catalyst and other

Pt alloy catalyst for the anode [15]. Another problem effect that requires a solution is the methanol crossover, which not only reduces the fuel utilization in the cell, but also contributes to the voltage loss in the cathode via a mixed potential. The membrane is the major control for methanol crossover. Although Nafion® (DuPont), the most frequently membrane used in DMFCs, poses high conductivity and stability, it suffers from high methanol crossover. Consequently, thicker versions of Nafion® (e.g. 117) are often used. Although thicker membranes reduce methanol crossover, they add more ohmic resistance. Therefore another major area of research is focused on the development of a methanol resistant membrane, including non-Nafion fluorinated membranes, composite fluorinated membranes, non-fluorinated membranes [16-18], and composite Nafion/PVA membranes [58].

Research directions have also concentrated in the development of mathematical models to understand the design parameters and the effect of the operating conditions in DMFCs. Extensive work in this area can be found in the literature and has been reviewed by several authors [17, 19-23]. The vast majority of these models are developed using a one-dimensional, steady state, isothermal, and single phase approach. Also, many models focused on the overall performance of the DMFC or are validated using only full-cell polarization data [24-30]. Some models are used to investigate in-depth a specific key area of the DMFC. These studies include the anode polarization [31-33], methanol crossover [34-37], with some authors separating the of electro-osmotic and diffusion fluxes [34, 37], and the effect of mixed potential in the cathode [38-40].

Yang, et al. investigated methanol and air flow rates to develop a model on the relationship between DMFC operating parameters and performance measures based on

equations developed in previous work. Sub-models looked at ohmic overpotential, open circuit voltage, and the total overpotential, while the semi-empirical model calculated coefficient values through numerical data fitting. Although the model was found to be effective for predicting DMFC performance based on the influences of temperature, methanol concentration, methanol flow rate, and air flow rate, it was limited to the TekStak DMFC and does not provide coefficient values for a wide range of DMFCs [52].

Jeong et al., in an effort to reduce fuel consumption and enable DMFCs to operate more efficiently, developed a model based on modifications of Sundmacher et al. and Zhou et al., which focuses on the entire operating procedure. Steady-state cell performance was determined based on the feed concentration of methanol, and a dynamic simulation verified the behavior of the DMFC from start-up to shut-down operation. Residual methanol fuel waste occurred in shut-down operation where the anode reaction rate drops. The model developed, which formulates the optimization problem as a non-linear programming problem, maximizes the performance of the DMFC under a given power density load [53].

Oliveira et al. looked at different parameters and their influence on the net water transport coefficient, yet another challenge in DMFC performance optimization. Low coefficient values were obtained when cathode air humidification was increased, as well as during decreases in membrane thickness and increases in the catalyst loading. The resulting model provides useful information for future high concentration or pure methanol DMFC systems [54].

In yet another analysis of performance losses within the DMFC, Escudero-Cid et al. looked at the degradation of a synthesized PtCoRu/C cathode compared to a Pt/C

cathode during short- and long-term cell operations. Rotating disk electrode studies showed that, in the presence of methanol, the oxygen reduction reaction performance is greatly affected with the use of the Pt/C cathode, whereas the PtCoRu/C cathode has only a minor affect. Electrochemistry impedance analysis also identified that the resistance associated to the anodic process increases with the severity of the overall degradation performance of the cells [55].

A more comprehensive analysis by Rosenthal et al. provides an isothermal model that accurately predicts experimental data established by Chiu et al. Based on an extensive list of parameters, the model provided for a good fit with data from Chiu et al. when looking at the effect of methanol feed concentration on DMFC performance. The model was also used to study the predicted methanol crossover current density at different operating temperatures, as well as to predict cathode and anode polarization. By controlling the methanol feed concentration, the model could be used to develop optimal operating condition control algorithms [56].

More recently, Casalegno et al. have looked at the dependence of methanol crossover on operating conditions and on membrane and gas diffusion layer (GDL) characteristics, such as morphology, thickness, PTFE content, and presence of a hydrophobic mictroporous layer at the cathode side and/or the anode side. Through experimental and modeling analyses, Casalegno et al. determined that methanol crossover decreases considerably in continuous operation [59], CO_2 measurement at the cathode is a reliable indicator of crossover, cathode feeding has very slight effects on crossover, and taking advantage of vapor methanol transport for the electrochemical reaction can have an effect on reducing crossover [60].

Many theoretical DMFC models have been developed to cover a broad range of performance optimization. However, little attention has been given to understand the individual voltage losses in the cell simultaneously with methanol crossover. This thesis presents a strategy to couple mathematical simulations with anode and cathode half-cell experiments, methanol crossover data, and hydrogen pump experiments to quantify individual losses in a DMFC. This approach breaks down the fuel cell losses and correlates the results with the parts of the model for each of the reaction elements to show the relation to the whole cell performance. A 1D analytical model was used in order to make quick predictions of the data, and experimental conditions were selected for which this model is applicable. The batch of tests prescribed allows not only the anode and cathode overpotentials to be quantified, but also for estimation of the voltage and fuel losses due to crossover of methanol. The model also captures the effect of cathode flow rate on methanol crossover and performance.

CHAPTER 2

MODEL DESCRIPTION

2.1 Voltage Loss Analysis

The cell voltage for a DMFC can be divided into voltages resulting from the anode, cathode, and membrane-electrode assembly (MEA) resistances, and is written as:

$$V_{Cell} = \left(U_{O_2} + \eta_{O_2} + \eta_{X-over}\right) - \left(U_{MeOH} + \eta_{MeOH}\right) - I_{Cell}\left(R_M + R_{Ion}\right) \qquad [1]$$

This equation suggests that these individual terms can be measured separately using anode half-cell, cathode half-cell, and hydrogen-pump experiments. It also assumes that the individual losses do not interact. For example, the methanol reaching the cathode creates a mixed cathode overpotential but does not affect the oxygen kinetics. The model parameters specific to these experiments can then be estimated and used in the full-cell model to predict cell performance as a function of operating conditions (e.g., current, methanol concentration, flow rates). The methodology and the assumptions made are discussed below.

The voltage measured in an anode half-cell experiment ($V_{A,exp}$) can be expressed as:

$$V_{A,exp} = \left(U_{MeOH} + \eta_{MeOH}\right) - \left(U_{H_2} + \eta_{H_2,red}\right) + I_{Cell}\left(R_M + R_{Ion}\right) \qquad [2]$$

The voltage measured in the hydrogen pump experiment ($V_{IR,exp}$) can be expressed as:

$$V_{IR,exp} = \left(U_{H_2} + \eta_{H_2,ox}\right) - \left(U_{H_2} + \eta_{H_2,red}\right) + I_{Cell}\left(R_M + R_{Ion}\right) \qquad [3]$$

The voltage measured in the cathode half-cell experiment ($V_{C,exp}$) can be expressed as:

$$V_{C,exp} = \left(U_{O_2} + \eta_{O_2}\right) - \left(U_{H_2} + \eta_{H_2,ox}\right) - I_{Cell}\left(R_M + R_{Ion}\right) \quad [4]$$

From Eq. [3] it can be see that the results from the hydrogen pump experiment gives not only the MEA resistance ($R_M + R_{Ion}$), but also the overpotentials for hydrogen oxidation and reduction. However, these terms are small since the kinetics for these reactions are facile. In addition, when data from the hydrogen-pump experiment are subtracted from the anode-half cell data, the result is:

$$V_{A,exp} - V_{IR,exp} - U_{MeOH} = \eta_{MeOH} - \eta_{H_2,ox} \quad [5]$$

where the overpotential for hydrogen reduction is eliminated. Therefore, the left hand side of Eq. [5] underestimates the anode overpotential value by the hydrogen oxidation overpotential. Again, this error is expected to be small relative to the error in the data and parameters estimation. The anode half-cell data is then fit to the following kinetic methanol oxidation expression [41]:

$$j = ai_{0,ref}^{MeOH} \frac{kc_{MeOH}^{A}}{c_{MeOH}^{A} + \lambda e^{\frac{\alpha_A F}{RT}\eta_{MeOH}}} e^{\frac{\alpha_A F}{RT}\eta_{MeOH}} \quad [6]$$

Similarly, the overpotential of the cathode can be estimated by the equation:

$$V_{C,exp} + V_{IR,exp} - U_{O_2} = \eta_{O_2} - \eta_{H_2,red} \quad [7]$$

Again, the left hand side of Eq. [7] underestimates the absolute value of the cathode overpotential, but the error introduced is expected to be small. The cathode half-cell data is then fit to the following Tafel expression:

$$i_{O_2} = i_{0,ref}^{O_2} \frac{c_{O_2}}{c_{O_2,ref}} \mathrm{e}^{-\frac{\alpha_C F}{RT}\eta_{O_2}} \quad [8]$$

2.2 Methanol Mass Transport

The mathematical model developed previously [1, 34] was modified to include the effect of mass transfer resistance in the anode and the unreacted methanol transport through the cathode on cell performance and methanol crossover. Specifically, the mass transfer resistance between the anode flow channel and the ABL was estimated using an empirical expression for flow in rectangular channel from Newman and Thomas-Alyea [42].

$$\mathrm{Sh} = 1.6151\left(\frac{\mathrm{ScRe}}{\ell_{Ch}/D_H}\right)^{1/3} - 1.2 - 0.28057\left(\frac{\ell_{Ch}/D_H}{\mathrm{ScRe}}\right)^{1/3} + O\left(\frac{\ell_{Ch}/D_H}{\mathrm{ScRe}}\right)^{2/3} \quad [9]$$

where the Sherwood, Reynold, and Schmidt numbers are defined respectively as:

$$\mathrm{Sh} = \frac{k_{Ch} D_H}{D_{MeOH}} \quad [10]$$

$$\mathrm{Re} = \frac{D_H v \rho}{\mu} \quad [11]$$

$$\mathrm{Sc} = \frac{\mu}{\rho D_{MeOH}} \quad [12]$$

The O in the last term of Eq. [9] indicates order of magnitude of the quantity in parenthesis.

From the dimensions of the flow channel, the hydraulic diameter can be determined as follows:

$$D_H = \frac{4A_{Cross}}{P_{Wet}} = \frac{2w_{Ch}\delta_{Ch}}{\left(w_{Ch} + \delta_{Ch}\right)} \quad [13]$$

For the model simulations the properties of the solution and the geometry of the flow channel are constant; only the velocity changes. Therefore, Eqs. [9] to [12] can be rearranged to give:

$$k_{Ch} = C_1 v^{\frac{1}{3}} - C_2 - C_3 v^{\frac{-1}{3}} + O\left(C_4 v^{\frac{-2}{3}} \right) \quad [14]$$

where

$$C_1 = 1.6151 \left(\frac{D_H^2}{D_{MeOH} \ell_{Ch}} \right)^{1/3} \quad [15]$$

$$C_2 = 1.2 \frac{D_{MeOH}}{D_H} \quad [16]$$

$$C_3 = 0.28057 \left(\frac{D_{MeOH} \ell_{Ch}}{D_H^2} \right)^{1/3} \quad [17]$$

$$C_4 = \left(\frac{D_{MeOH} \ell_{Ch}}{D_H^2} \right)^{2/3} \quad [18]$$

This mass transfer resistance between the anode flow channel and the ABL is in series with the resistance of the ABL. Therefore, an additional resistance ($1/k_{Ch}$) is added to the resistance of the ABL (δ_B / D_B) in the previous model [1]. Otherwise, the equations governing the anode are the same.

The methanol crossover is controlled by diffusion and electroosmotic drag through the membrane and is given as [1]:

$$N_{MeOH,z}^{M} = \frac{D_M \left(c_{II} - c_{III} \right)}{\delta_M} + \xi_{MeOH} \frac{i_{Cell}}{F} \quad [19]$$

where c_{II} and c_{III} are the methanol concentrations at anode and cathode side of the membrane as shown in Figure 2.1. As it will be shown later, the gas flow in the cathode changes the methanol diffusion flux through the membrane by affecting c_{III}. Consequently, c_{III} is used as an adjustable parameter in the model in order to fit the methanol crossover data. However, this concentration can be expressed as a fraction, β, of the methanol concentration at z_{II} as follows:

$$c_{III} = \beta c_{II} \qquad [20]$$

Combining Eqs. [19] and [20] gives:

$$N^{M}_{MeOH,z} = \frac{D_M (1-\beta) c_{II}}{\delta_M} + \xi_{MeOH} \frac{i_{Cell}}{F} \qquad [21]$$

Thus, $1-\beta$ represents the fraction of methanol concentration that drops across the membrane. At open circuit the electroosmotic flux term in Eq. [21] is zero, and there is no consumption of methanol in the ACL.

$$c_{II} \approx c^{Ch}_{MeOH} \qquad [22]$$

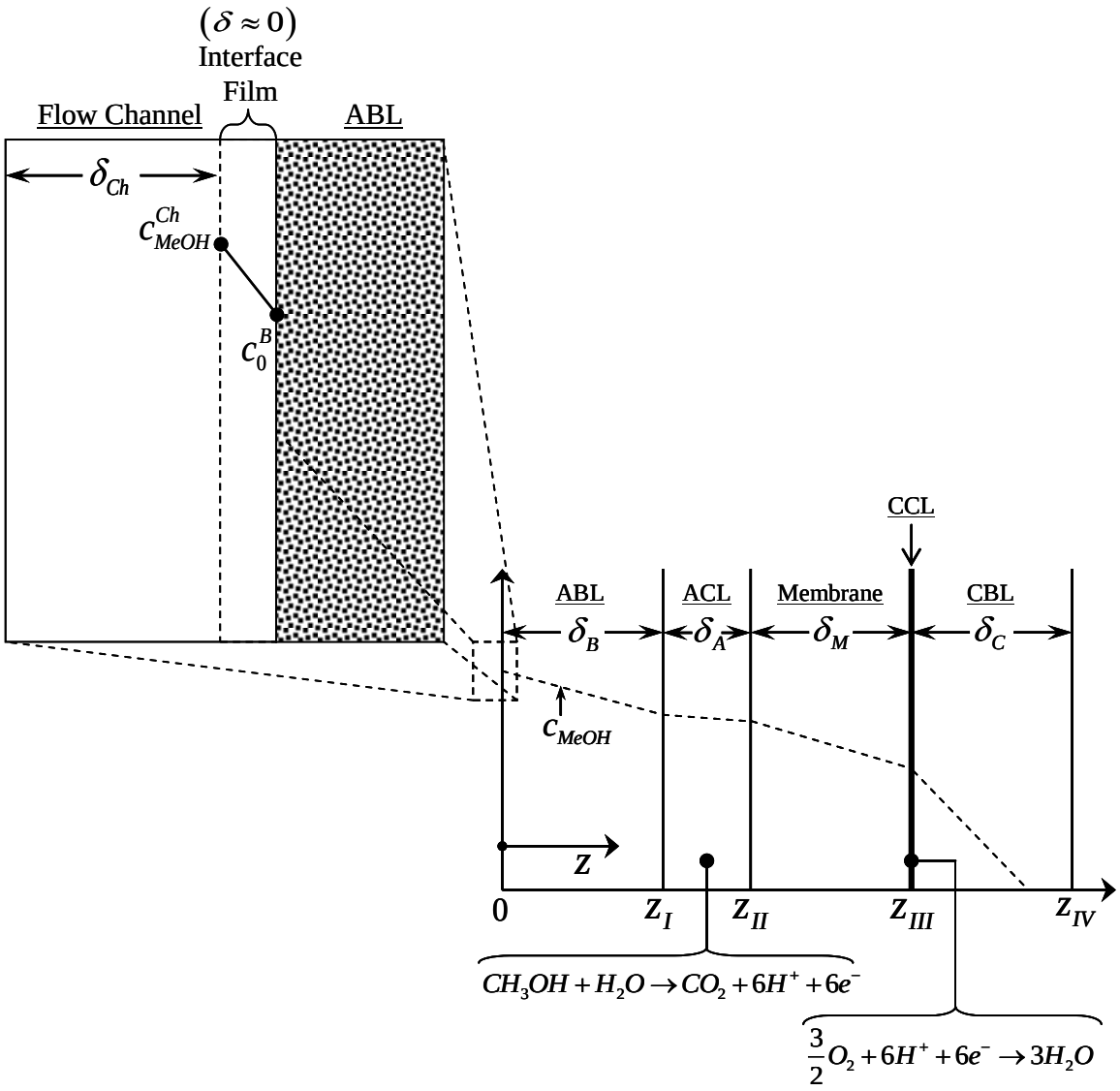

Figure 2.1: Schematic of the DMFC layers considered in the model showing the resistance at the anode flow channel – backing layer interface.

Consequently, by measuring the methanol crossover at open circuit for different methanol concentration it is possible to determine β from the slope of $N^{M}_{MeOH,z}$ vs c^{Ch}_{MeOH}.

The leakage current due to methanol oxidation in the cathode catalyst layer is given by

$$i_{Leak} = 6F\left(N^{M}_{MeOH,z} - N^{C}_{MeOH,z}\right) \quad [23]$$

In Eq. [23], the unreacted methanol is calculated as

$$N^{C}_{MeOH,z} = k_C c_{III} \quad [24]$$

where k_C is the mass transfer coefficient. As discussed above, at open circuit the electroosmotic flux term in Eq. [19] is zero. Also, since there is no reaction in the anode and the cathode, Eq. [22] holds true and

$$N^{M}_{MeOH,z} = N^{C}_{MeOH,z} \quad [25]$$

Therefore, combining the first term of Eq. [19] with Eqs. [22], [24], and [25] gives:

$$k_C = \left(\frac{c^{Ch}_{MeOH}}{N^{M}_{MeOH,z}} - \frac{\delta_M}{D_M}\right)^{-1} \quad [26]$$

Using Eq. [26], the mass transfer coefficient was determined from measurements of methanol crossover at open circuit as function of cathode flow rate for different concentrations. This does not mean that the flux of unreacted methanol is the same at open circuit than it is under load. Rather, assuming that k_C is the same under load than it is at open circuit just means that the resistance to mass transfer is the same under the two conditions.

A portion of the methanol crossing the membrane is oxidized at the cathode. This is the leakage current defined by Eq. [23]. Coupling the measured total methanol

crossover to the kinetics given in Eq. [8] enables an accurate estimate of the overpotential caused by crossover as:

$$\eta_{X-over} = -\frac{RT}{\alpha_C F}\ln\left(\frac{c_{O_2,ref} i_{Leak}}{c_{O_2} i_{0,ref}^{O_2}}\right) \quad [27]$$

The value of η_{X-over} estimated from Eq. [27] can be used with Eq. [1] to approximate the full-cell voltage.

CHAPTER 3

EXPERIMENTAL

3.1 Cell Preparation

Tests were performed using a fuel cell of 25 cm^2 from Fuel Cell Technologies. The membrane electrode assembly (MEA) was constructed with a Nafion® 117 membrane and E-TEK gas diffusion electrodes prepared according to the decal method of Wilson [43]. The anode loading was 3 mg/cm^2 of 40 wt% 1:1 PtRu/C catalyst and the cathode loading was 5 mg/cm^2 of 40wt% Pt/C. Tests were conducted using an 890C load cell from Scribner Associates Inc. with a methanol fuel system and the software package FuelCell® (Scribner Associates Inc.) was used to control the station. The membrane was hydrated with water for 24 hours with a 40 ccm flow of water in the anode and a 20 sccm flow of oxygen at 2 atm (absolute) in the cathode. The cell temperature and inlet temperatures were 70°C. All reagents were certified as ultra high purity.

3.2 DMFC Testing

For the full-cell polarization, the cell was operated as shown in Figure 3.1. Prior to running tests with a given concentration of methanol, the system was flushed with 1.5 L of methanol solution. The flow rate in the anode was set to maintain a 20 stoichiometric excess ratio with a minimum flow rate of 2 sccm. The flow rate in the cathode was set to maintain a 20 stoichiometric excess ratio with a minimum flow rate of

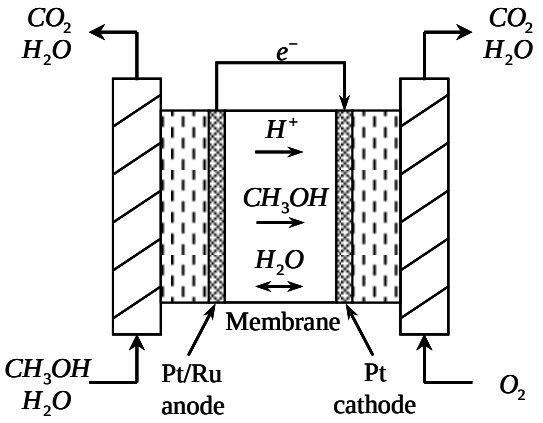

Anode: $CH_3OH + H_2O \rightarrow CO_2 + 6H^+ + 6e^-$

Cathode: $\frac{3}{2}O_2 + 6H^+ + 6e^- \rightarrow 3H_2O$

Cathode parasitic reaction: $CH_3OH + H_2O \rightarrow CO_2 + 6H^+ + 6e^-$

Overall: $\frac{3}{2}O_2 + CH_3OH \rightarrow CO_2 + 2H_2O$

Figure 3.1: Schematic of a DMFC.

20 sccm. These conditions were selected such that the 1D analytical model approach is valid. Polarization curves between 0.2 V and open circuit were run at constant voltage and the current was allowed to equilibrate at each condition for 15 minutes before recording the current.

3.3 Anode Half-Cell Testing

For the anode half-cell polarization, the cell was operated as a methanol electrolysis cell as shown in Figure 3.2. At the anode, methanol and water were oxidized to CO_2, protons and electrons. At the cathode, protons were reduced to form hydrogen. Hydrogen also flowed through this electrode to serve as a reference electrode. The flow rates of methanol and hydrogen were set to be the same as the flow rates of methanol and oxygen during a full-cell test, respectively. An HP 6032A (Hewlett-Packard) DC power source was used to apply a current between the anode and cathode. The voltage necessary to maintain a specific current was measured by the power supply and checked using a digital multimeter. The limiting current was determined when the voltage necessary to maintain a particular current reached 1 V.

3.4 Hydrogen Pump Testing

A hydrogen pump experiment was run by switching the terminals on the power supply while running the cells in the setup for the anode half cell experiment. A diagram of the experimental setup for the hydrogen pump test is shown in Figure 3.3. At the anode (the cathode under anode half-cell conditions), hydrogen was oxidized to protons and electrons. At the cathode, protons were reduced to form hydrogen back. The flow rates of

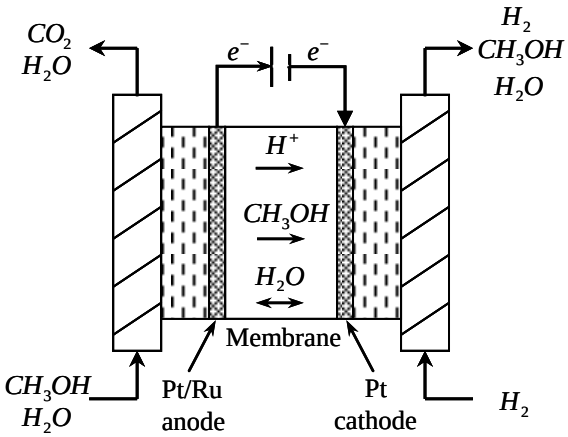

Anode: $CH_3OH + H_2O \rightarrow CO_2 + 6H^+ + 6e^-$

Cathode: $6H^+ + 6e^- \rightarrow 3H_2$

Overall: $CH_3OH + H_2O \rightarrow CO_2 + 3H_2$

Figure 3.2: Schematic of the anode half cell.

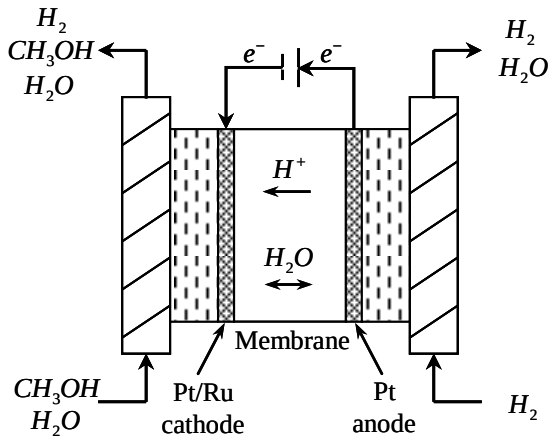

Anode: $H_2 \rightarrow 2H^+ + 2e^-$

Cathode: $2H^+ + 2e^- \rightarrow H_2$

Overall: $H_2 \rightarrow H_2$

Figure 3.3: Schematic of the hydrogen pump cell.

methanol and hydrogen were set to be the same as the flow rates of methanol and oxygen during a full-cell test, respectively.

3.5 Cathode Half-Cell Testing

For cathode half-cell polarization, the cell was run similar to a PEMFC with a hydrogen anode and an oxygen cathode. Figure 3.4 shows a diagram of the cathode half-cell experimental setup. Dry oxygen was flowed through the cathode at the same stoichiometry as for the full-cell DMFC experiments. In the anode, saturated hydrogen with a dewpoint of 80°C was flowed at a stoichiometry of 4. Condensing conditions were used to simulate the environment in a DMFC where liquid water in the anode saturates the membrane. High stoichiometric flow was used to minimize concentration overpotential in the anode.

3.6 Methanol Crossover

The methanol crossover was determined by measuring the amount of CO_2 in the cathode exhaust. In the analysis of the crossover experiments, the measured CO_2 comes from the methanol that is oxidized at the cathode as described by the parasitic reaction shown in Figure 3.1 and the unreacted methanol that is oxidized in the gas chromatograph (GC). Gas samples from the cathode outlet were collected using a SGE GAV-200 gas sampler after condensed water was removed from the line. A GC Buck Scientific model 910 equipped with a molecular sieve 5A column was used to measure the CO_2 concentration from the gas samples. The volumetric flow rate of the gas at the cathode outlet was measured using a digital bubble flowmeter Agilent Optiflow 650.

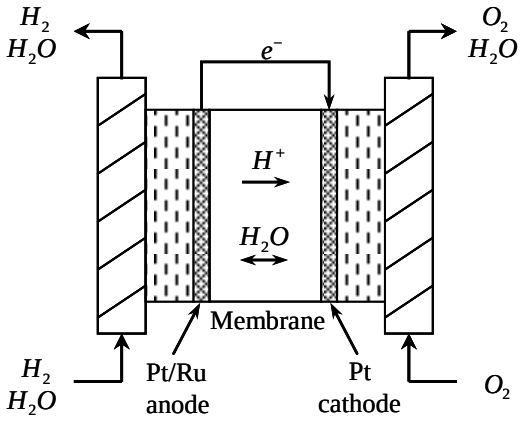

Anode: $H_2 \rightarrow 2H^+ + 2e^-$

Cathode: $\frac{1}{2}O_2 + 2H^+ + 2e^- \rightarrow H_2O$

Overall: $H_2 + \frac{1}{2}O_2 \rightarrow H_2O$

Figure 3.4: Schematic of the cathode half cell.

CHAPTER 4

RESULTS AND DISCUSSION

The methanol crossover reported in the literature is commonly based on cells that use a constant flow in the cathode. However, this work addresses the difference between constant stoichiometry and constant flow on methanol crossover. This is important because the cathode flow affects the methanol crossover as shown in Figure 4.1. This figure shows the methanol crossover at open circuit as function of cathode flow. Since no electroosmotic drag exists at open circuit, the increase in the methanol crossover observed in the figure is due to increased concentration gradient across the MEA. At higher cathode flow rates, the methanol concentration gradient has reached a maximum and thus the methanol transport by diffusion has as well.

As discussed previously, the mass transfer coefficient was calculated from Eq. [26] and using the measured methanol crossover as function of cathode flow rate from Figure 4.1. The results were fitted to the following equation:

$$k_C = \left(-7x10^{-13}\right)Q_C^3 - \left(2x10^{-11}\right)Q_C^2 + \left(1x10^{-6}\right)Q_C \qquad [28]$$

where Q_C is the inlet volumetric flow rate at the cathode flow channel.

As described in the experimental section, the full-cell polarization and the individual voltage losses were measured under the same conditions. The parameters used

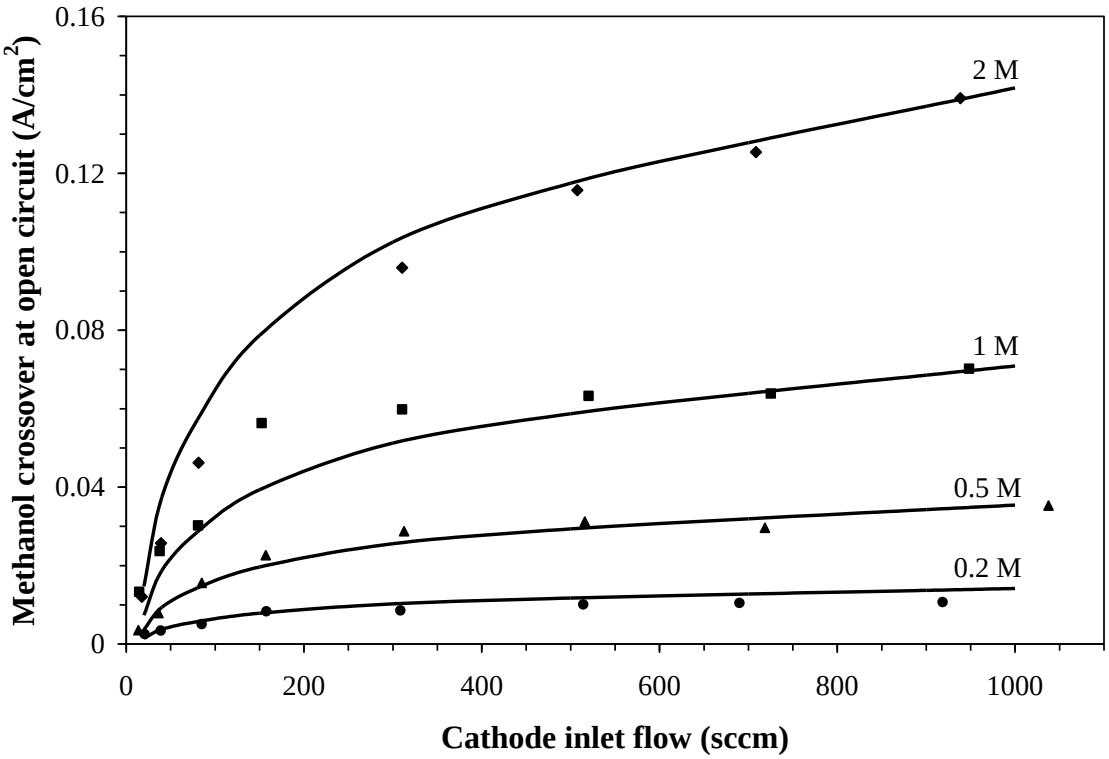

Figure 4.1: Methanol crossover at open circuit as function of the inlet cathode flow rate with model simulations (lines) for different methanol concentrations.

to fit the model to data are shown in Table 4.1. Model parameters were chosen using literature values and from fitting the experimental data. In Eq. [6], $i_{0,ref}^{MeOH}$ was obtained from Wang and Wang [24] while the parameters a, k, λ, and α_A were used to fit the anode half-cell data. In addition, the methanol diffusion coefficients in the anode backing layer (ABL) and anode catalyst layer (ACL), D_B and D_A respectively, affect the methanol concentration at the ACL, c_{MeOH}^{A}. These values are critical in the mass transfer limited region for either the anode half-cell and full-cell polarizations. Consequently, D_B and D_A were estimated in order to fit the limiting current density from the anode half-cell and the full-cell polarizations. In Eq.[8], $i_{0,ref}^{O_2}$ was obtained from Parthasarathy et al. [44] while α_C was used to fit the cathode half-cell data. In Eq. [19], the diffusion coefficient of methanol, D_M, is obtained from Scott et al.[45] and the electroosmotic drag coefficient is obtained from Ren et al.[46]

The experimental full-cell polarization results obtained at 343 K using different methanol concentrations are shown in Figure 4.2 with model predictions of the experimental data. The results show that the cell with 1 M produces a power around 25 mW/cm^2 at 0.5 V. This performance is below the optimum seen in literature but is a reasonable value for a DMFC. The model is able to predict the cell polarizations for concentrations of methanol between 0.05 M and 2.0 M. However, the model appears to show the most error in predicting the mass transfer limitations for the higher methanol concentrations.

Table 4.1. Model parameters used throughout

Parameter	Value	Reference or Experimental Data Fitted
ak	0.75 cm^{-1}	Anode half-cell & full polarization
D_A	$2.3x10^{-5}\ \frac{cm^2}{s}$	Anode half-cell & full polarization
D_B	$1.85x10^{-5}\ \frac{cm^2}{s}$	Anode half-cell & full polarization
D_M	$4.9x10^{-6}e^{2436\left(\frac{1}{333}-\frac{1}{T}\right)}\ \frac{cm^2}{s}$	Scott et al.[45]
$i_{0,ref}^{MeOH}$	$9.425x10^{-3}e^{\frac{35570}{R}\left(\frac{1}{353}-\frac{1}{T}\right)}\ \frac{A}{cm^2}$	Wang and Wang[24]
$i_{0,ref}^{O_2}$	$4.222x10^{-3}e^{\frac{73200}{R}\left(\frac{1}{353}-\frac{1}{T}\right)}\ \frac{A}{cm^2}$	Parthasarathy et al.[44]
ℓ_{Ch}	155 cm	-----
$R_M + R_{Ion}$	14.2 mΩ	H_2 pump
T	343.15 K	-----
U_{MeOH}^0	0.03 V	Wang and Wang[24]
$U_{O_2}^0$	1.24 V	Wang and Wang[24]
w_{Ch}	0.08 cm	-----
α_A	0.64	Anode half-cell & full polarization
α_C	0.94	Cathode half-cell & full polarization
β	0.94	MeOH crossover at OCV
δ_A	0.0025 cm	-----
$\delta_B = \delta_C$	0.028 cm	-----
δ_{Ch}	0.1 cm	-----
δ_M	0.018 cm	-----
λ	$5.8x10^{-9}$ mol/cm^3	Anode half-cell & full polarization
ξ_{MeOH}	$4x_{MeOH}$	Ren et al.[46]

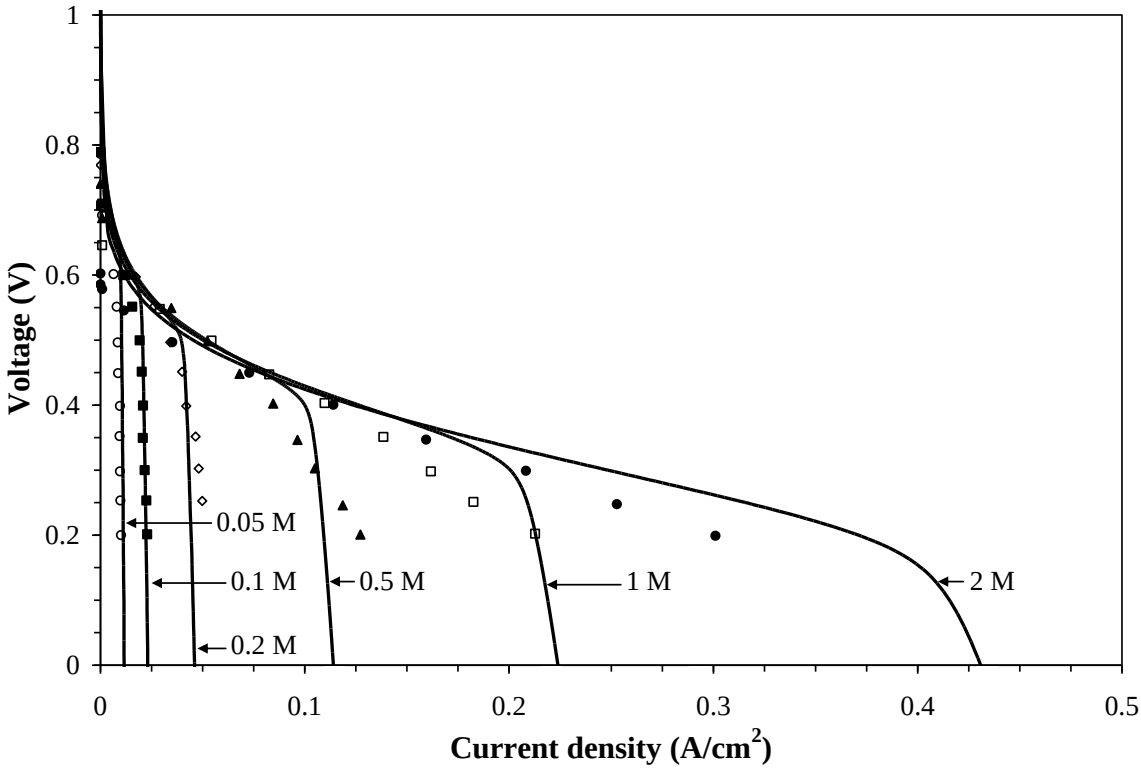

Figure 4.2: Experimental cell polarization (symbols) and model simulations (lines) for different methanol concentrations.

Figure 4.3 shows the anode overpotential using different methanol concentrations. The anode overpotential was obtained by correcting the anode polarization data for the ohmic potential drop and the proper thermodynamic reference as shown in the left hand side of Eq. [5]. Then the data was fitted using Eq. [6]. Although k and λ affect the anode overpotential curve, it is α_A that shows a significant effect. The model has the most error in predicting the behavior for the cell near the mass transfer limited region for high concentrations of methanol. The error of the model in this region could be due to formation of CO_2 bubbles that could alter the mass-transfer in this region.

The cell voltage during the hydrogen pump experiment is shown in Figure 4.4. If the losses due to hydrogen oxidation and reduction are small, the slope obtained from a linear regression of the hydrogen pump data gives an approximation of the ohmic resistance in the membrane and electrode ionomer. The resistance obtained from these experiments was used to calculate the amount of voltage drop caused by the ionomer and membrane.

The absolute value of the cathode overpotential is shown in Figure 4.5. The cathode overpotential was obtained by correcting the cathode polarization data for the ohmic potential drop and the proper thermodynamic reference as shown in the left hand side of Eq. [7]. Then the data was fitted using Eq. [8]. Using a similar approach to the anode, the higher cathode overpotential observed for cell 2 was fitted by using a lower α_C in Eq. [8]. This overpotential is the overpotential of the cathode without the mixed

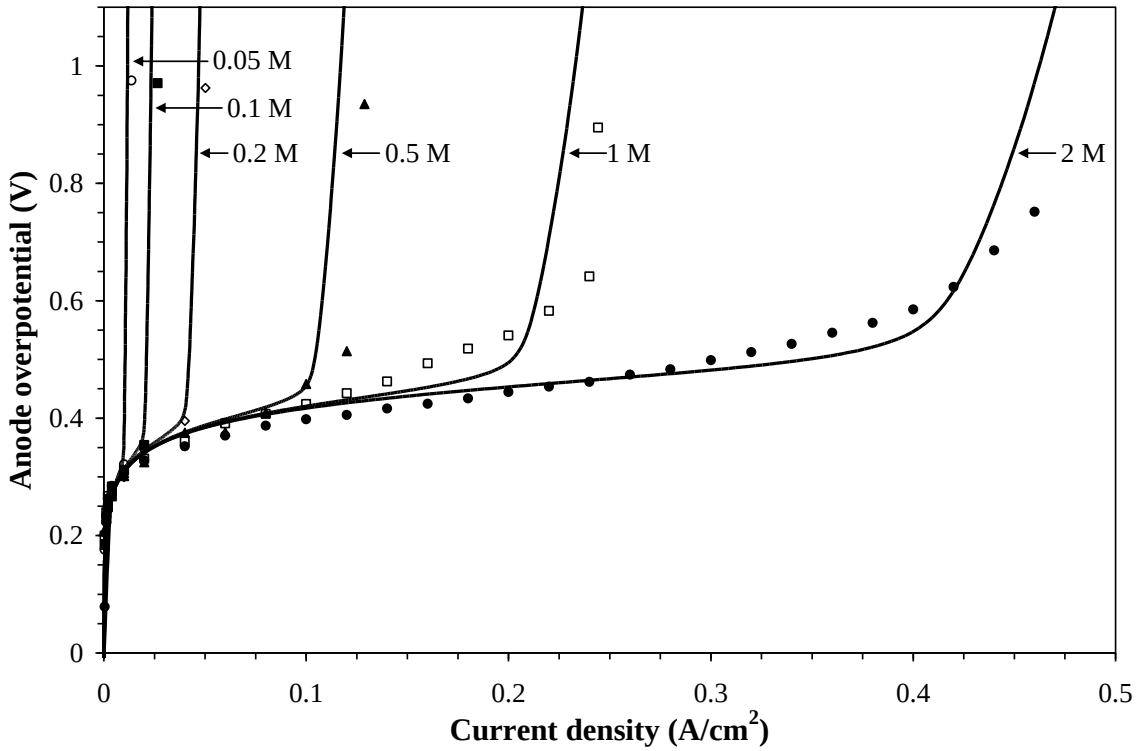

Figure 4.3: Experimental anode polarizations (symbols) and model simulations (lines) for different methanol concentrations.

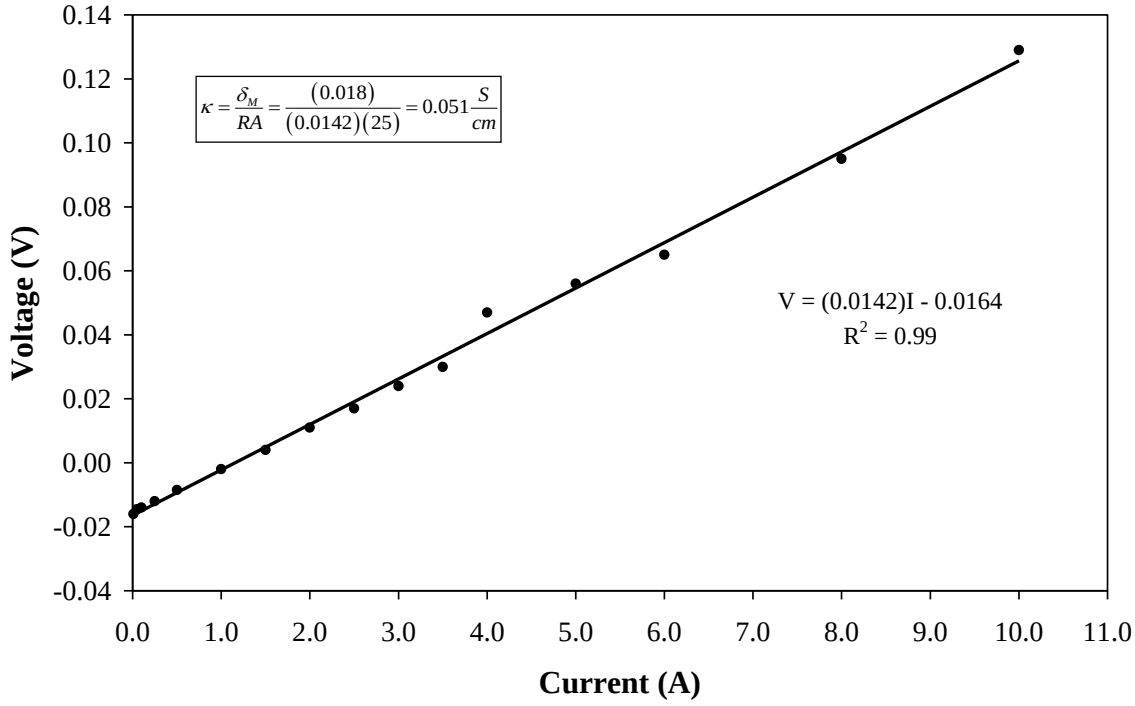

Figure 4.4: Voltage response as function of current for the hydrogen pump experiment.

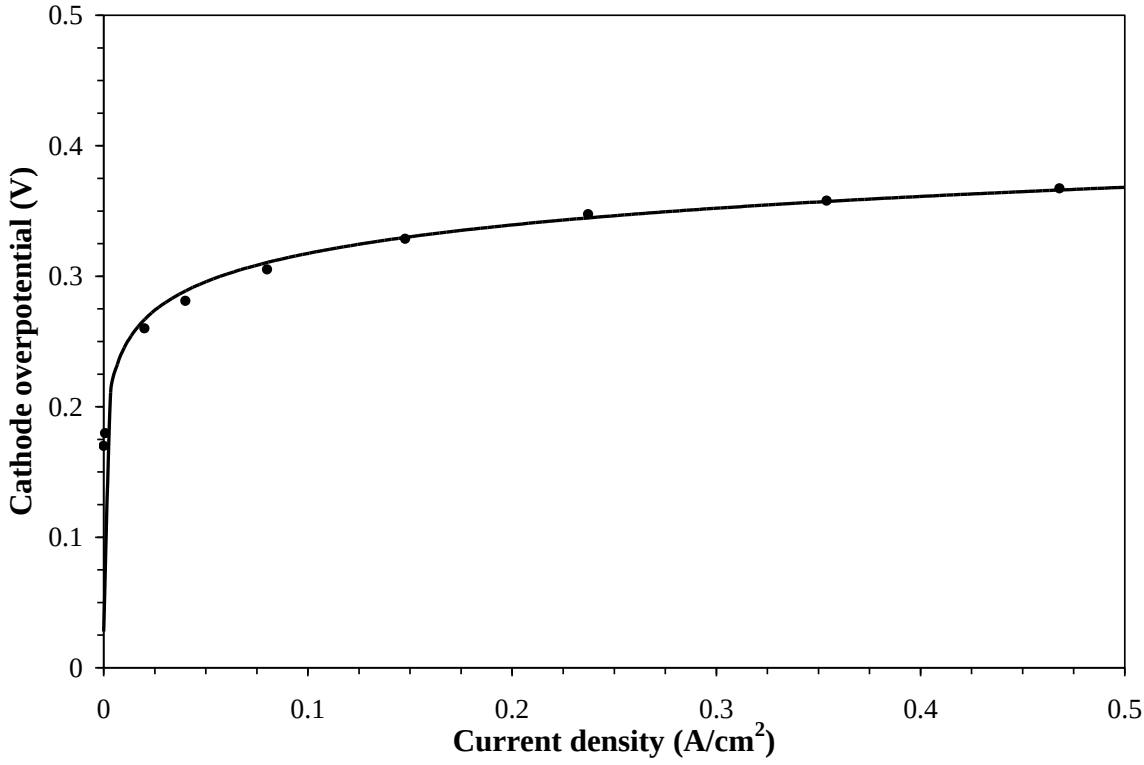

Figure 4.5: Experimental cathode polarization (symbols) and model simulation (line).

potential effect caused by the crossover of methanol. Cyclic voltammetry experiments performed on the cathode during the cathode half-cell experiments showed no signs of residual CO adsorbed to the cathode catalyst.

During the measurement of CO_2 in the cathode to determine methanol crossover, it has been argued that CO_2 coming from the anode can interfere with the measurements [47-49]. To quantify the amount of CO_2 crossover in the cell, crossover measurements were taken during anode half-cell experiments. The amount of CO_2 measured was very small compared to the total CO_2 measured in the full cell experiment to determine the methanol crossover. Although as much as 20% error has been found in the leakage current by neglecting CO_2 crossover [34], the compression pressure of the cells used in this work is 1380 kPa as compared to the cell used in Eccarius et al. [34] which has a significant lower compression pressure of 285 kPa. The high compression in the cell can significantly affect the crossover as will be discussed later. Consequently, in this work the CO_2 effect from the anode was neglected for determining the methanol crossover.

At open circuit the methanol crossover is only by diffusion, and the slope of the line of $N^{M}_{MeOH,z}$ vs c^{Ch}_{MeOH} shown in Figure 4.6 is used to determine $\beta = 0.94$. Consequently, c_{III} is 94% of c_{II} which means there is only a 6% drop of methanol concentration across the membrane.

The predictions of the methanol crossover for different methanol concentrations are compared to experimental crossover measurements in Figure 4.7. These plots of

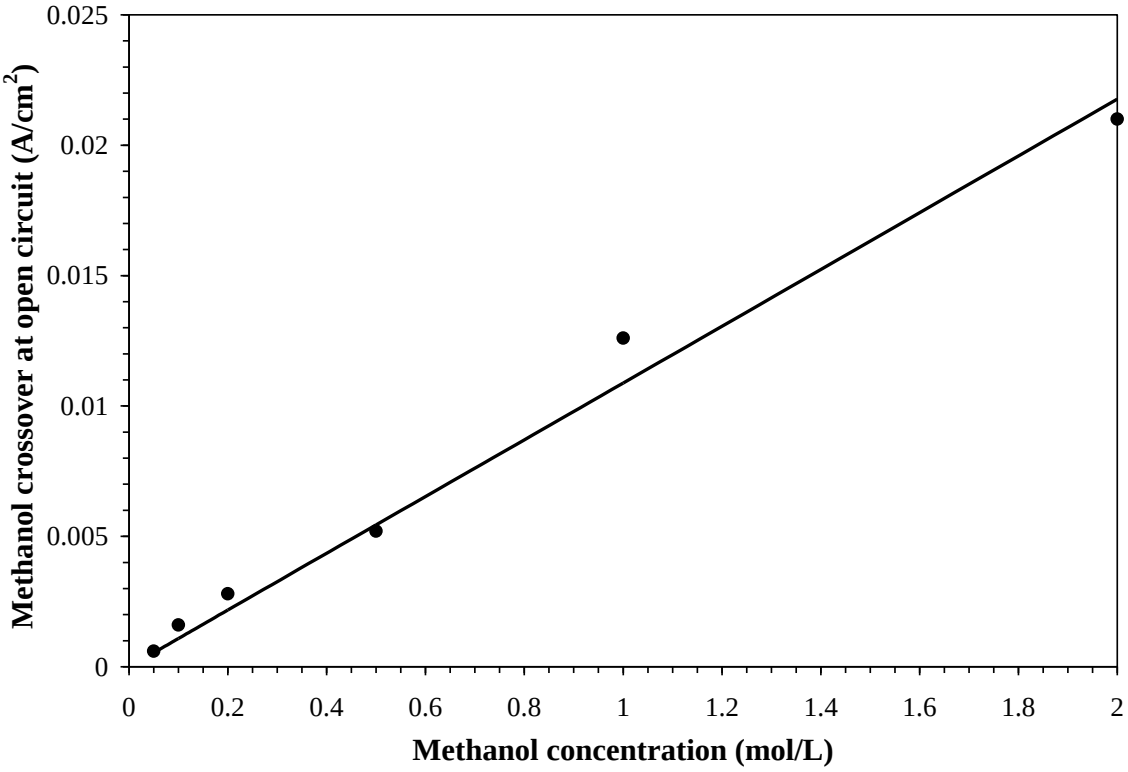

Figure 4.6: Methanol crossover at open circuit as function of methanol concentration with model simulation (line).

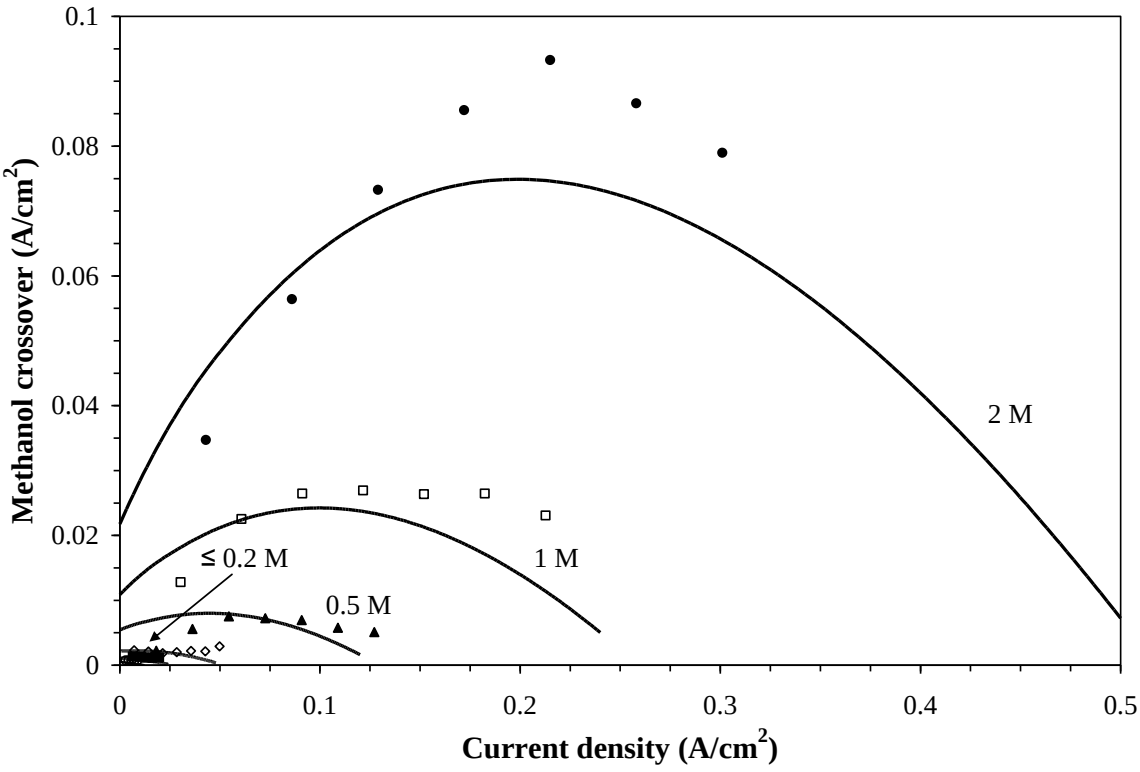

Figure 4.7: Experimental methanol crossover (symbols) and model simulations (lines) for different methanol concentrations.

methanol crossover are generally parabolic in shape and show a maximum in the crossover current at intermediate current densities. The maximum in crossover current is seen because electroosmotic drag, rather than diffusion, is the primary transport mechanism for methanol through the membrane. This is illustrated in Figure 4.8 for the case of 1 M methanol.

Typical methanol crossover curves shown in literature do not show a maximum in the crossover current [47, 49-51]. Conversely, they show a monotonically decreasing methanol crossover with increasing current, which suggest diffusion is the primary transport mechanism. Diffusion rates are affected by cell compression, cathode catalyst layer thickness, cathode flow rate, or a combination of these parameters.

To understand the effect of cell compression, methanol crossover measurements at open circuit were performed using the cell described in the experimental section (cell 1), which has an internal compression pressure of 1380 kPa, and another cell with identical conditions (cell 2), except that it is compressed to 480 kPa. Results show a methanol crossover equivalent to 63 and 185 mA/cm^2 for the cells 1 and 2 respectively. In this case, the decrease in cell compression allows higher diffusion of methanol through the membrane. However, the performance of cell 2 was not significantly lower than the performance of cell 1.

In addition to cell compression, the effect of cathode catalyst loading in the methanol crossover was studied. It was observed that generally the methanol crossover

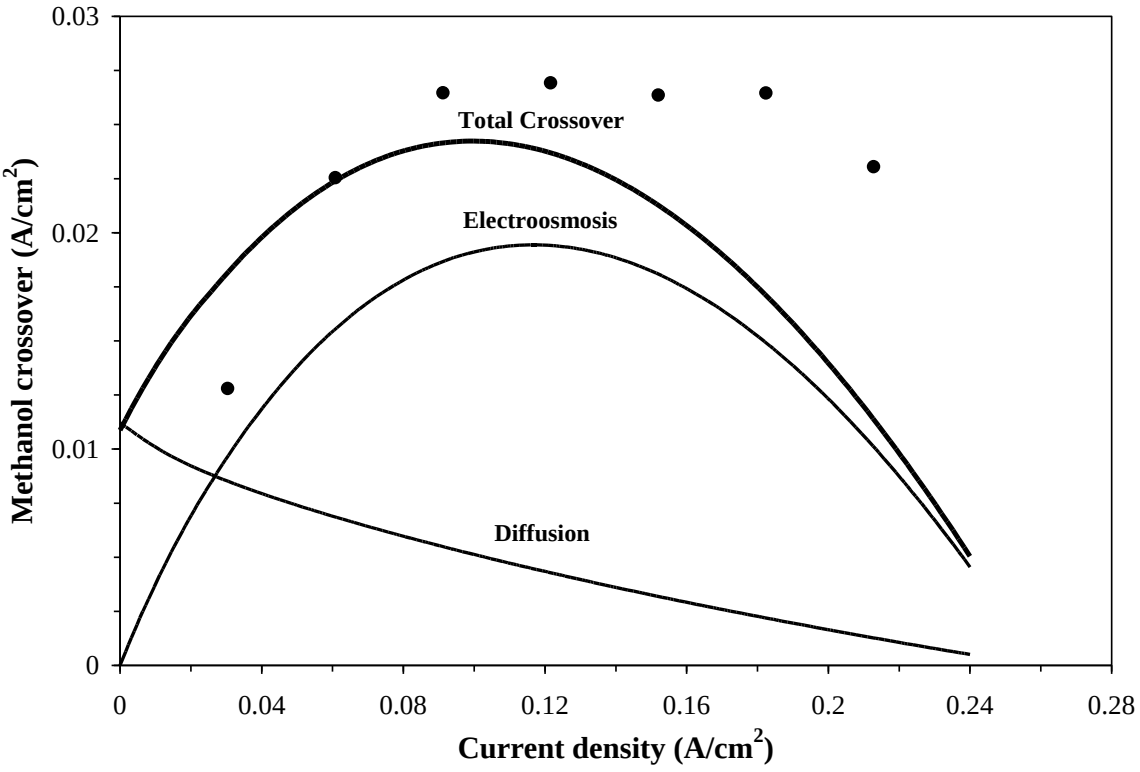

Figure 4.8: Methanol crossover for 1 M methanol at a constant stoichiometry of 20 in the cathode.

decreases as the cathode catalyst loading increases. This effect can be explained by the fact that the cathode catalyst layer thickness increases with loading. A thicker cathode catalyst layer will increase the resistance to methanol diffusion and hence decreases the methanol crossover through the membrane. The high cathode catalyst loading used in this work, as well as the high cell compression, contribute to the lower methanol crossover observed in Figure 4.7 as compared to the literature.

With all the kinetic and transport processes quantified, the cell voltage can be deconstructed. For example, using the previous experimental data for the case of 1 M methanol, it is possible to account for the individual losses in order to provide further understanding about the cell performance as shown in Figure 4.9. The thermodynamic value for the DMFC is 1.21 V. The anode overpotential, the ohmic drop in the membrane and electrode ionomer, the overpotential of the cathode, and the loss due to crossover are subtracted from 1.21 V to obtain the polarization curve. The final curve represents the calculated cell polarization which matches the experimental polarization curve. It can be observed that the anode overpotential accounts for most of the losses in the cell followed by the cathode overpotential. The losses from crossover can be seen to be relatively small and only contribute significantly to the cell losses near open circuit. The voltage loss from methanol crossover would increase if a high flow rate is used in the cathode.

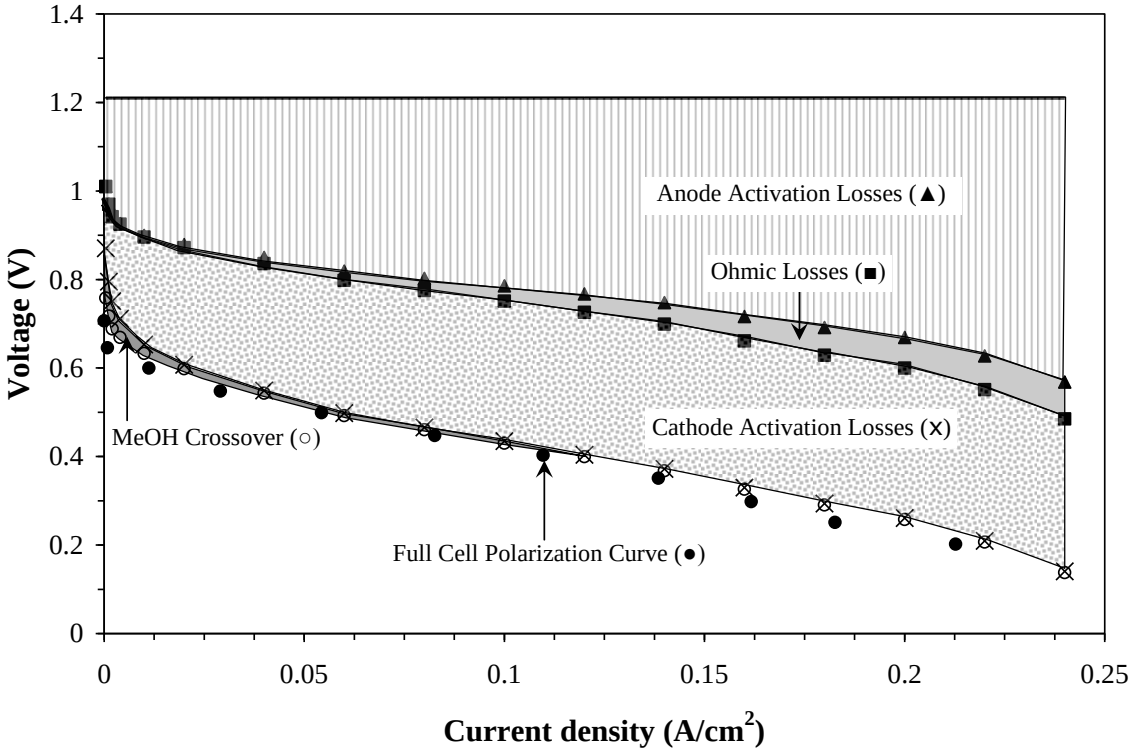

Figure 4.9: Individual voltage losses from cell polarization with 1 M methanol concentration.

CHAPTER 5

CONCLUSIONS

The one-dimensional model, developed previously, was improved by including: (1) methanol transport from the anode flow channel to the backing layer using a mass transfer resistance; and (2) accounting for the unreacted methanol transport through the cathode. These improvements enable the effect of cathode flow rate on cell voltage and methanol crossover to be predicted.

Cathode flow rate has been shown to affect the methanol crossover by diffusion. Cells operated at constant stoichiometry, or where the cathode flow rate is small, can show a parabolic shape in the methanol crossover due to the electroosmotic drag dominance over diffusion as the primary transport mechanism for methanol through the membrane. Conversely, sufficient high cathode flow rate will increase the methanol transport by diffusion which can dominates the electroosmotic drag of methanol through the membrane. This will make the methanol crossover curves more linear in shape.

By using anode half-cell, cathode half-cell, hydrogen pump, and methanol crossover experiments, the individual losses in a DMFC were investigated. The individual voltage losses for a cell operated at 343 K with an O_2 cathode at 2 atm absolute pressure accounted for all of the voltage loss observed during the operation of the full cell. The anode activation accounted for most of the losses in the cell followed by the cathode activation. The model was able to reasonably predict the anode, cathode, full-cell

polarization, and methanol crossover data for methanol concentrations between 0.05 M and 2 M at all operating currents. The ability to identify individual losses allows for better analysis of losses in the catalyst layer and allow for more effective catalyst optimization. Future research on fuel cells can benefit from this model by analyzing the performance of other fuel cells, identifying where the individual voltage losses are occurring, and optimizing the performance of said cells in each voltage loss area.

REFERENCES

[1] García, B. L., Sethuraman, V. A., Weidner, J. W., White, R. E., and Dougal, R., 2004, "Mathematical Model of a Direct Methanol Fuel Cell," Journal of Fuel Cell Science and Technology, 1(1), pp. 43-48.

[2] Wasmus, S., and Kuver, A., 1999, "Methanol Oxidation and Direct Methanol Fuel Cells: A Selective Review," Journal of Electroanalytical Chemistry, 461(1-2), pp. 14-31.

[3] Schultz, T., Zhou, S., and Sundmacher, K., 2001, "Current Status of and Recent Developments in the Direct Methanol Fuel Cell," Chemical Engineering & Technology, 24(12), pp. 1223-1233.

[4] Mcgrath, K. M., Prakash, G. K. S., and Olah, G. A., 2004, "Direct Methanol Fuel Cells," Journal of Industrial and Engineering Chemistry, 10(7), pp. 1063-1080.

[5] Liu, H. S., Song, C. J., Zhang, L., Zhang, J. J., Wang, H. J., and Wilkinson, D. P., 2006, "A Review of Anode Catalysis in the Direct Methanol Fuel Cell," Journal of Power Sources, 155(2), pp. 95-110.

[6] Loffler, M. S., Natter, H., Hempelmann, R., and Wippermann, K., 2003, "Preparation and Characterisation of Pt-Ru Model Electrodes for the Direct Methanol Fuel Cell," Electrochimica Acta, 48(20-22), pp. 3047-3051.

[7] Garcia, B. L., Captain, B., Adams, R. D., Hungria, A. B., Midgley, P. A., Thomas, S. J. M., and Weidner, J. W., 2007, "Bimetallic Cluster Provides a Higher Activity

Electrocatalyst for Methanol Oxidation," Journal of Cluster Science, 18(1), pp. 121-130.

[8] Du, H. D., Li, B. H., Kang, F. Y., Fu, R. W., and Zeng, Y. Q., 2007, "Carbon Aerogel Supported Pt-Ru Catalysts for Using as the Anode of Direct Methanol Fuel Cells," Carbon, 45(2), pp. 429-435.

[9] Garcia, B. L., Fuentes, R., and Weidner, J. W., 2007, "Low-Temperature Synthesis of a Ptru/Nb0.1ti0.9o2 Electrocatalyst for Methanol Oxidation," Electrochemical and Solid State Letters, 10(7), pp. B108-B110.

[10] Zainoodin, A. M., Kamarudin, S. K., and Daud, W. R. W., 2010, "Electrode in Direct Methanol Fuel Cells," International Journal of Hydrogen Energy, 35(10), pp. 4606-4621.

[11] Kim, M. S., Fang, B., Chaudhari, N. K., Song, M., Bae, T. S., and Yu, J. S., 2010, "A Highly Efficient Synthesis Approach of Supported Pt-Ru Catalyst for Direct Methanol Fuel Cell," Electrochimica Acta, 55(15), pp. 4543-4550.

[12] Daimon, H., Onodera, T., Nakagawa, T., Nitani, H., and Yayamoto, T. A., 2010, "Methanol Oxidation Activity of Nanosized Ptru Catalysts and Their Microstructures," Journal of Nanoelectronics and Optoelectronics, 5(2), pp. 120-124.

[13] Arico, A. S., Antonucci, P. L., Modica, E., Baglio, V., Kim, H., and Antonucci, V., 2002, "Effect of Pt-Ru Alloy Composition on High-Temperature Methanol Electro-Oxidation," Electrochimica Acta, 47(22-23), pp. 3723-3732[14] Dickinson, A. J., Carrette, L. P. L., Collins, J. A., Friedrich, K. A., and Stimming, U., 2004, "Performance of Methanol Oxidation Catalysts with Varying Pt : Ru Ratio as a Function of Temperature," Journal of Applied Electrochemistry, 34(10), pp. 975-980.

[15] Serov, A., and Kwak, C., 2009, "Review of Non-Platinum Anode Catalysts for Dmfc and Pemfc Application," Applied Catalysis B-Environmental, 90(3-4), pp. 313-320.

[16] Heinzel, A., and Barragan, V. M., 1999, "A Review of the State-of-the-Art of the Methanol Crossover in Direct Methanol Fuel Cells," Journal of Power Sources, 84(1), pp. 70-74.

[17] Deluca, N. W., and Elabd, Y. A., 2006, "Polymer Electrolyte Membranes for the Direct Methanol Fuel Cell: A Review," Journal of Polymer Science Part B-Polymer Physics, 44(16), pp. 2201-2225.

[18] Neburchilov, V., Martin, J., Wang, H. J., and Zhang, J. J., 2007, "A Review of Polymer Electrolyte Membranes for Direct Methanol Fuel Cells," Journal of Power Sources, 169(2), pp. 221-238.

[19] Wang, C. Y., 2004, "Fundamental Models for Fuel Cell Engineering," Chemical Reviews, 104(10), pp. 4727-4765.

[20] Sousa, R., and Gonzalez, E. R., 2005, "Mathematical Modeling of Polymer Electrolyte Fuel Cells," Journal of Power Sources, 147(1-2), pp. 32-45.

[21] Oliveira, V. B., Falcao, D. S., Rangel, C. M., and Pinto, A., 2007, "A Comparative Study of Approaches to Direct Methanol Fuel Cells Modelling," International Journal of Hydrogen Energy, 32(3), pp. 415-424.

[22] Garcia, B. L., and Weidner, J. W., 2007, Modern Aspects of Electrochemistry, Springer-Verlag New York, LLC, New York, Review of Direct Methanol Fuel Cells.

[23] Zhao, T. S., Xu, C., Chen, R., and Yang, W. W., 2009, "Mass Transport Phenomena in Direct Methanol Fuel Cells," Progress in Energy and Combustion Science, 35(3), pp. 275-292.

[24] Wang, Z. H., and Wang, C. Y., 2003, "Mathematical Modeling of Liquid-Feed Direct Methanol Fuel Cells," Journal of the Electrochemical Society, 150(4), pp. A508-A519.

[25] Argyropoulos, P., Scott, K., Shukla, A. K., and Jackson, C., 2003, "A Semi-Empirical Model of the Direct Methanol Fuel Cell Performance - Part I. Model Development and Verification," Journal of Power Sources, 123(2), pp. 190-199.

[26] Guo, H., and Ma, C., 2004, "2d Analytical Model of a Direct Methanol Fuel Cell," Electrochemistry Communications, 6(pp. 306-312.

[27] Miao, Z., He, Y. L., Li, X. L., and Zou, J. Q., 2008, "A Two-Dimensional Two-Phase Mass Transport Model for Direct Methanol Fuel Cells Adopting a Modified Agglomerate Approach," Journal of Power Sources, 185(2), pp. 1233-1246.

[28] Yan, T. Z., and Jen, T. C., 2008, "Two-Phase Flow Modeling of Liquid-Feed Direct Methanol Fuel Cell," International Journal of Heat and Mass Transfer, 51(5-6), pp. 1192-1204.

[29] He, Y. L., Li, X. L., Miao, Z., and Liu, Y. W., 2009, "Two-Phase Modeling of Mass Transfer Characteristics of a Direct Methanol Fuel Cell," Applied Thermal Engineering, 29(10), pp. 1998-2008.

[30] Zou, J. Q., He, Y. L., Miao, Z., and Li, X. Y., 2010, "Non-Isothermal Modeling of Direct Methanol Fuel Cell," International Journal of Hydrogen Energy, 35(13), pp. 7206-7216.

[31] Baxter, S. F., Battaglia, V. S., and White, R. E., 1999, "Methanol Fuel Cell Model: Anode," Journal of the Electrochemical Society, 146(2), pp. 437-447.

[32] Shivhare, M. R., Jackson, C. L., Scott, K., and Martin, E. B., 2007, "Simplified Model for the Direct Methanol Fuel Cell Anode," Journal of Power Sources, 173(1), pp. 240-248.

[33] Casalegno, A., and Marchesi, R., 2008, "Dmfc Anode Polarization: Experimental Analysis and Model Validation," Journal of Power Sources, 175(1), pp. 372-382.

[34] Eccarius, S., García, B. L., Hebling, C., and Weidner, J. W., 2008, "Experimental Validation of a Methanol Crossover Model in Dmfc Applications," Journal of Power Sources, 179(pp. 723-733.

[35] Yin, K. M., 2008, "A Theoretical Model of the Membrane Electrode Assembly of Liquid Feed Direct Methanol Fuel Cell with Consideration of Water and Methanol Crossover," Journal of Power Sources, 179(2), pp. 700-710.

[36] Casalegno, A., and Marchesi, R., 2008, "Dmfc Performance and Methanol Cross-Over: Experimental Analysis and Model Validation," Journal of Power Sources, 185(1), pp. 318-330.

[37] Kareemulla, D., and Jayanti, S., 2009, "Comprehensive One-Dimensional, Semi-Analytical, Mathematical Model for Liquid-Feed Polymer Electrolyte Membrane Direct Methanol Fuel Cells," Journal of Power Sources, 188(2), pp. 367-378.

[38] Kulikovsky, A. A., 2005, "On the Nature of Mixed Potential in a Dmfc," Journal of the Electrochemical Society, 152(6), pp. A1121-A1127.

[39] Chen, C. H., and Yeh, T. K., 2006, "A Mathematical Model for Simulating Methanol Permeation and the Mixed Potential Effect in a Direct Methanol Fuel Cell," Journal of Power Sources, 160(2), pp. 1131-1141.

[40] Liu, F. Q., and Wang, C. Y., 2007, "Mixed Potential in a Direct Methanol Fuel Cell - Modeling and Experiments," Journal of the Electrochemical Society, 154(6), pp. B514-B522.

[41] Meyers, J. P., and Newman, J., 2002, "Simulation of the Direct Methanol Fuel Cell - Ii. Modeling and Data Analysis of Transport and Kinetic Phenomena," Journal of the Electrochemical Society, 149(6), pp. A718-A728.

[42] Newman, J., and Thomas-Alyea, K. E., 2004, *Electrochemical Systems*, John Wiley & Sons, Inc., New Jersey.

[43] Wilson, M. S., 1993, U.S. Pat. 5,211,984.

[44] Parthasarathy, A., Srinivasan, S., Appleby, A. J., and Martin, C. R., 1992, "Temperature Dependence of the Electrode Kinetics of Oxygen Reduction at the Platinum/Nafion Interface - a Microelectrode Investigation," Journal of the Electrochemical Society, 139(9), pp. 2530-2537.

[45] Scott, K., Taama, W., and Cruickshank, J., 1997, "Performance and Modelling of a Direct Methanol Solid Polymer Electrolyte Fuel Cell," Journal of Power Sources, 65(1-2), pp. 159-171.

[46] Ren, X. M., Springer, T. E., Zawodzinski, T. A., and Gottesfeld, S., 2000, "Methanol Transport through Nafion Membranes - Electro-Osmotic Drag Effects on Potential Step Measurements," Journal of the Electrochemical Society, 147(2), pp. 466-474.

[47] Dohle, H., Divisek, J., Merggel, J., Oetjen, H. F., Zingler, C., and Stolten, D., 2002, "Recent Developments of the Measurement of the Methanol Permeation in a Direct Methanol Fuel Cell," Journal of Power Sources, 105(2), pp. 274-282.

[48] Drake, J. A., Wilson, W., and Killeen, K., 2004, "Evaluation of the Experimental Model for Methanol Crossover in Dmfcs," Journal of the Electrochemical Society, 151(3), pp. A413-A417.

[49] Gogel, V., Frey, T., Zhu, Y. S., Friedrich, K. A., Jorissen, L., and Garche, J., 2004, "Performance and Methanol Permeation of Direct Methanol Fuel Cells: Dependence on Operating Conditions and on Electrode Structure," Journal of Power Sources, 127(1-2), pp. 172-180.

[50] Hikita, S., Yamane, K., and Nakajima, Y., 2002, "Influence of Cell Pressure and Amount of Electrode Catalyst in Mea on Methanol Crossover of Direct Methanol Fuel Cell," Jsae Review, 23(1), pp. 133-135.

[51] Jiang, R. Z., and Chu, D. R., 2004, "Comparative Studies of Methanol Crossover and Cell Performance for a Dmfc," Journal of the Electrochemical Society, 151(1), pp. A69-A76.

[52] Yang, Q., Kianimanesh, A., Freiheit, T., Park, S.S., and Xue, D., 2011, "A Semi-Empirical Model Considering the Influence of Operating Paramters on Performance for a Direct Methanol Fuel Cell," Journal of Power Sources, 196(X), pp 10640-10651.

[53] Jeong, I., Kim, J., Pak, S., Woo Nam, S., and Moon, I., 2008, "Optimum Operating Strategies for Liquid-Fed Direct Methanol Fuel Cells," Journal of Power Sources, 185(1), pp. 828-837.

[54] Oliveira, V.B., Rangel, C.M., and Pinto, A.M.F.R., 2009, "Water Management in Direct Methanol Fuel Cells," International Journal of Hydrogen Energy, 34(X), pp. 8245-8256.

[55] Escudero-Cid, R., Hernandez-Fernandez, P., Perez-Flore, J.C., Rojas, S., Garcia-Rodriguez, S., Fatas, E., and Ocon, P., 2011, "Analysis of Performance Losses of Direct Methanol Fuel Cell with Methanol Tolerant PtCoRu/C Cathode Electrode," International Journal of Hydrogen Energy, 37, pp. 7119-7130.

[56] Rosenthal, N.S., Vilekar, S.A., and Datta, R., 2012, "A Comprehensive Yet Comprehensible Analytical Model for the Direct Methanol Fuel Cell," Journal of Power Sources, 206, pp. 129-143.

[57] Garcia-Diaz, B.L., Patterson, J.R., Weidner, J.W., 2012, "Quantifying Individual Losses in a Direct Methanol Fuel Cell,", Journal of Fuel Science and Tecnhology, 9(1), pp. 011012-1-9.

[58] Molla, Sergio., Compan, Vicente., 2011, "Performance of Composite Nafion/PVA Membranes for Direct Methanol Fuel Cells," Journal of Power Sources, 196, pp. 2699-2708.

[59] Casalegno, A., Bresciani, M., Zago, M., Marchesi, R., 2014, "Experimental Investigation of Methanol Crossover Evolution During Direct Methanol Fuel Cell Degradation Tests," Journal of Power Sources, 249, pp. 103-109.

[60] Casalegno, A., Santoro, C., Rinaldi, F., Marchesi, R., 2011, "Low Methanol Crossover and High Efficiency Direct Methanol Fuel Cell: The Influence of Diffusion Layers," Journal of Power Sources, 196, pp. 2669-2675.